https://doi.org/10.5194/egusphere-2023-1791
Preprint. Discussion started: 17 August 2023

How a volcanic arc influences back-arc extension: insight from 2D numerical models

Duo Zhang[1] and Huw Davies[1]

[1]School of Earth and Environmental Sciences, Cardiff University, Cardiff, CF10 3AT, the UK

Correspondence: Duo Zhang (zhangd27@cardiff.ac.uk)

Abstract. Investigating plate tectonics through the lens of back-arc extension in subduction systems, this study introduces a 'hot region' on the overriding plate (OP) in 2D thermo-mechanical models, simulating the role of an arc. Two extension locations on the OP were identified by the models: at the hot region (Mode EH) or surprisingly at a far-field location which is about 750 km from the trench (Mode EF). The study also found that extension could occur at the same far-field location without a hot region when the OP is young and thin, or the subducting plate (SP) is old and strong. Our models suggest that EH mode is common, occurring in many cases like Mariana Trough and Lau Basin, while the EF mode is rare, potentially occurring in scenarios like the Japan Sea. The primary driving mechanism in our models is poloidal flow beneath the OP, and the extension process is the competition of basal drag which thins the OP versus thermal healing which thickens it, and also a competition of thermal weakening at the hot region and at the far-field location. Increased trench retreat rates, facilitated by increased hot region temperature and width, encouraged this flow and consequently promoted back-arc extension.

1 Introduction

Back-arc extension is the first stage of the formation of a back-arc basin (BAB) which is found at the rear of an arc on the overriding plate (OP) in a subduction system. It provides a significant window into plate tectonics by displaying both convergent and divergent margins.

The driving mechanisms of back-arc extension have been widely explored by laboratory and numerical modeling (Duarte et al., 2013; Schellart and Moresi, 2013; Clio and Pieter, 2013; Bettina et al., 2014; Holt et al., 2015; Chen et al., 2016; Sheng et al., 2019; Dal Zilio et al., 2018; Wolf and Huismans, 2019; Erdős et al., 2022). Numerous factors that influence back-arc extension have been investigated, including plate ages (Capitanio et al., 2011; Sheng et al., 2019; Dasgupta et al., 2021), slab width (Schellart and Moresi, 2013; Magni et al., 2014), slab dip (Lallemand et al., 2005; Dasgupta et al., 2021), negative buoyancy of the slab (Chen et al., 2015), etc. Most of the previous models concentrated on the effect of the subducting plate (SP) which has been identified as a driving force for mantle flow and plate tectonics (Schellart, 2004), but only a few studies have explored the role that OP properties play in back-arc extension (Clio and Pieter, 2013). Moreover, the majority of the models listed above include a homogeneous OP, which eliminates the impact that possible weak regions (such as previous suture zones or volcanic arcs) may have on the results. There are a few numerical studies that introduce inherited weak zones

https://doi.org/10.5194/egusphere-2023-1791
Preprint. Discussion started: 17 August 2023

on the OP by lowering the viscosity directly (Nakakuki and Mura, 2013; Dal Zilio et al., 2018; Yang et al., 2019, 2021), but they primarily focus on simulating 'suture zones' on the continental lithosphere.

Even though BABs are all referred to as 'back'-arc basins, most of them were formed by breaking volcanic island arcs apart, leaving a remnant arc on the other side of the basin, such as Lau Basin which was formed by splitting Tonga Ridge and Lau Ridge apart (Zellmer and Taylor, 2001), Havre Trough between Kermadec Ridge and Colville Arc, Mariana Trough between Mariana Arc and West Mariana Ridge, etc. This phenomenon demonstrates that the presence of a volcanic arc can be important for constraining the location of extension, but few studies have taken this into account Bettina et al. (2014). To investigate this further, we have in this study run a series of 2-D thermo-mechanical and self-consistently driven models with a hot region that simulates a thermal volcanic arc on the OP. We will interchangeably use the terms volcanic arc / arc / hot zone knowing that readers understand that this is shorthand for approximating the effect of an arc with a hot zone. Firstly, we tested a series of models which have homogeneous OPs without arcs for comparison. Then, an arc was introduced into the OP to investigate its role in back-arc extension. We aim to look into how an arc influences back-arc extension and its position.

A remaining issue is that the properties of a volcanic arc are not very well known. Even though the location of present-day arcs is known from the Smithsonian Global Volcanism Project database, the arc-trench distances range widely from 2-1539 km data from Earthbyte, (Jodie, 2016). Additionally, the temperatures of arcs before their extension are difficult to constrain. Thus, we introduced a simplified model for the thermal signature of an arc, which allowed us to test a range of parameters for the arcs (including their width, arc-trench distance, and the central temperature anomaly) systematically to figure out their roles in back-arc extension.

2 Model description

Based on the work of Garel et al. (2014), a series of 2-D thermally-driven subduction models are run using the code Fluidity, a computational modeling framework suitable for geodynamic models, which uses an adaptive unstructured mesh that can be optimised dynamically (Davies et al., 2011). It provides a higher resolution in the region where the fields are changing most quickly spatially and a lower resolution in the regions where the field of the prognostic variable is stable and hardly changing. For example, in this 2D subduction model in a domain of 10,000 km by 2,900 km, adaptivity allows the model to have grid spacing ranging from 400 m near the subduction zone interface between the SP and OP, to 200 km in more quiescent regions in the deepest mantle. It is a significant advantage in that it retains the accuracy of the solution while reducing the calculation effort.

2.1 Model setup

A 2D thermo-mechanical model of the subduction system was built with a juxtaposed subducting plate (SP) and overriding plate (OP) by Garel et al. (2014). The model has a large domain to reduce the influence of boundary conditions, which is 10000 km in length and 2900 km (the whole mantle depth) in depth (Figure 1), and a thin weak layer lies on the SP and decouples the two plates to encourage the subduction of the SP. In the initial condition, the SP is set to bend beneath the OP with a radius

https://doi.org/10.5194/egusphere-2023-1791
Preprint. Discussion started: 17 August 2023

of curvature of 250 km, and the depth of the tip of SP is around 194 km, that is, the SP has already started subduction at the beginning of the model. In this way, the problem of subduction initiation is avoided. The two corners on the top surface represent ridges of the two plates, where the initial age is 0 Ma. The intersection of the plates is the position of the trench, where we set the initial age of plates as $AgeSP^0$ and $AgeOP^0$. The initial ages of plates have a linear change horizontally from 0 to $AgeSP^0$ and $AgeOP^0$. Velocity boundary conditions are free-slip on the bottom and the two sides, whereas the top boundary has a free surface (Kramer et al., 2012).

High heat flow has been observed in active volcanic arcs (Manga et al., 2012), so arcs can be expected to be described by a relatively high temperature. In the initial thermal structure, a hot region has been introduced on the OP to simulate the volcanic arc (Figure 1). The temperature at a chosen distance (from 100 to 1050 km) from the trench is increased by a certain degree (from 25 to 800 degrees) vertically from a prescribed depth to the surface. It cools off by a linear function over a prescribed horizontal distance (named 'Width', from 10 to 50 km) to merge in with the background temperature. The mantle temperature limits the maximum value, which is 1300°C. The hot region extends in depth from the surface to where it reaches the maximum temperature. The hot region has a higher temperature than the background, so its viscosity is lower as well (producing a pre-existing weak zone in the OP at the start of the simulation).

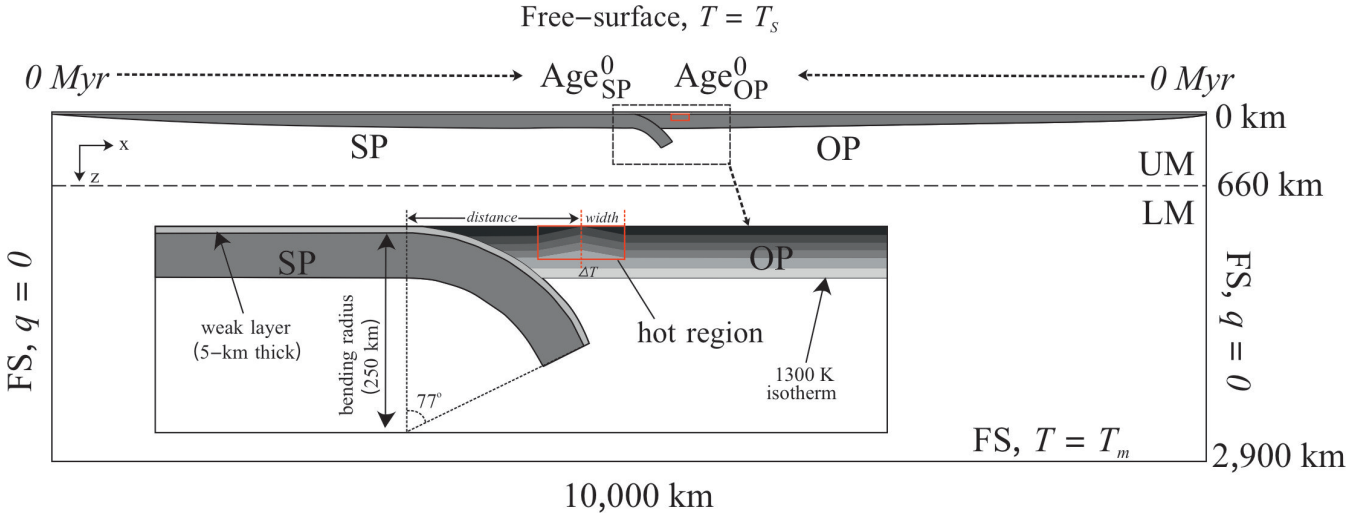

Figure 1. Model setup and initial geometry of the subduction simulations with the initial thermal structure of the hot region (modified from Garel et al. (2014)).

2.2 Governing equations

The governing equations of mantle dynamics follow the conservation law of mass, momentum, and energy. We solve the simplest set of equations by assuming an incompressible mantle and the Boussinesq approximation (McKenzie et al., 1974).

https://doi.org/10.5194/egusphere-2023-1791
Preprint. Discussion started: 17 August 2023

The momentum and continuity equations are

$$\partial_i u_i = 0, \tag{1}$$

$$\partial_i \sigma_{ij} = -\Delta\rho g_j = \alpha\rho_s \left(T - T_s\right) g_j, \tag{2}$$

and the evolution of the thermal field follows:

$$\frac{\partial T}{\partial t} + u_i \partial_i T = \kappa \partial_i^2 T, \tag{3}$$

In these three equations, κ denotes the thermal diffusivity, u_i and g_j are the vectors of velocity and gravity (which is oriented vertically downwards), respectively. In the $\Delta\rho$ (density anomaly term), T is the temperature, T_s is the temperature at the Earth's surface and ρ_s is the nominal density at T_s, α is the coefficient of thermal expansion, and σ_{ij} is the full stress tensor which can be decomposed into deviatoric and lithostatic components, according to

$$\sigma_{ij} = \tau_{ij} - p\delta_{ij}, \tag{4}$$

with τ_{ij} as the deviatoric stress tensor, p is dynamic pressure, and δ_{ij} is the Kronecker delta function.

τ_{ij} the deviatoric stress tensor and $\dot{\varepsilon}_{ij}$, the strain rate tensor are related by μ, the viscosity

$$\tau_{ij} = 2\mu\dot{\varepsilon}_{ij} = \mu\left(\frac{\partial u_i}{\partial x_j} + \frac{\partial u_j}{\partial x_i}\right), \tag{5}$$

2.3 Rheology

Four deformation processes of rocks that occur in the slab and mantle are considered: diffusion creep, dislocation creep, Peierls creep, and yielding. The first two mechanisms dominate the deformation at high temperatures, with diffusion creep being important in a low-stress environment, while dislocation creep is most significant under high stress. All of them are temperature-dependent except for yielding viscosity, and they have the following generic relationship with temperature, stress, activation energy, the prefactor, and strain rate:

$$\mu_{diff/disl/P} = A^{-\frac{1}{n}} exp\left(\frac{E + PV}{nRT_r}\right) \dot{\varepsilon}_{II}^{\frac{1-n}{n}}, \tag{6}$$

In this equation, A is a prefactor, n is the stress exponent with a value of 1, 3.5 and 20 for diffusion, dislocation and Peierls creep, respectively; E is the activation energy, from 250 to 300 kJ/mol in diffusion creep and from 400 to 550 kJ/mol in dislocation creep of the upper mantle, and it is smaller in the lower mantle; P is the lithostatic pressure, given by P=$\rho_s$gz, ρ_s is the reference density at the Earth's surface temperature T_s, g is the acceleration due to gravity and z is the depth; V is the activation volume, R is the gas constant, and $\dot{\varepsilon}_{II}$ is the second invariant of the strain rate tensor. Temperature (T), on which the rheology of slabs and mantle most depend, is given initially as

https://doi.org/10.5194/egusphere-2023-1791
Preprint. Discussion started: 17 August 2023

$$T(x,z,t=0) = T_s + (T_m - T_s)\, erf\left(\frac{z}{2\sqrt{\kappa Age^0(x)}}\right), \tag{7}$$

where z is the depth, x is the horizontal coordinate, and t is the time, T_s the temperature at Earth's surface and T_m the mantle temperature. T_r in equation (6) is the temperature in equation (7) adding an adiabatic gradient of 0.5 K/km in the upper mantle and 0.3 K/km in the lower mantle (Fowler et al., 1990).

In addition, the yielding viscosity is given by

$$\mu_y = \frac{\tau_y}{2\dot{\varepsilon}_{II}}, \tag{8}$$

with τ_y the yield strength:

$$\tau_y = min(\tau_y + f_c P, \tau_{y,max}), \tag{9}$$

τ_0 is the surface yield strength, f_c is the friction coefficient, P is the lithostatic pressure, and $\tau_{y,max}$ is the maximum yield strength.

The composite viscosity is based on the combination of these mechanisms via

$$\mu = \left(\frac{1}{\mu_{diff}} + \frac{1}{\mu_{disl}} + \frac{1}{\mu_y} + \frac{1}{\mu_P}\right)^{-1}. \tag{10}$$

This is assuming that all 4 deformation processes act in parallel. There are 2 materials set in our models, and the whole domain is controlled by similar rheological laws in both of them. The second material is in a weak (5 km thick) layer upon the subducting plate tracked down to 194 km depth, and graded out below 200 km depth. It is the same parameters as the other material covering virtually the whole domain, other than it has a very low friction coefficient (about one-tenth of that in the normal material), and a lower maximum viscosity of 10^{20} Pa s (10^{25} Pa s in normal material) to ensure the decoupling between the subducting and overriding plates. All the parameters of the model setup are listed in Table 1.

Table 1: Key parameters used in this research.

Quantity	Symbol	Units	Value
Gravity	g	$m\ s^{-2}$	9.8
Thermal expansivity coefficient	α	K^{-1}	3×10^{-5}
Thermal diffusivity	κ	$m^2\ s^{-1}$	10^{-6}
Reference density	ρ_s	$kg\ m^{-3}$	3300

https://doi.org/10.5194/egusphere-2023-1791
Preprint. Discussion started: 17 August 2023

Cold, surface temperature	T_s	K	273
Hot, mantle temperature	T_m	K	1573
mantle geothermal gradient	G	$\mathrm{K\ km^{-1}}$	0.5 (UM)
			0.3 (LM)
Gas constant	R	$\mathrm{J\ K^{-1}\ mol^{-1}}$	8.3145
Maximum viscosity	μ_{max}	Pa s	10^{25}
Minimum viscosity	μ_{min}	Pa s	10^{18}
Diffusion Creep			
Activation energy	E	$\mathrm{kJ\ mol^{-1}}$	300 (UM)
			200 (LM)
Activation volume	V	$\mathrm{cm^3\ mol^{-1}}$	4 (UM)
			1.5 (LM)
Prefactor	A	$\mathrm{Pa^{-n}\ s^{-1}}$	3.0×10^{-11} (UM)
			6.0×10^{-17}
	n		1
Dislocation Creep (UM)			
Activation energy	E	$\mathrm{kJ\ mol^{-1}}$	540
Activation volume	V	$\mathrm{cm^3\ mol^{-1}}$	12
Prefactor	A	$\mathrm{Pa^{-n}\ s^{-1}}$	5.0×10^{-16}
	n		3.5
Peierls Creep (UM)			
Activation energy	E	$\mathrm{kJ\ mol^{-1}}$	540
Activation volume	V	$\mathrm{cm^3\ mol^{-1}}$	10
Prefactor	A	$\mathrm{Pa^{-n}\ s^{-1}}$	10^{-150}
	n		20
Yield Strength Law			
Surface yield strength	τ_0	MPa	2
Friction coefficient	f_c		0.2
	$f_{c,weak}$		0.02 (weak layer)
Maximum yield strength	$\tau_{y,max}$	MPa	10,000

https://doi.org/10.5194/egusphere-2023-1791
Preprint. Discussion started: 17 August 2023

3 Results

Two sets of models with a hot region were run to test the role of properties of a hot region (Table A1) and plate ages (Table A2), respectively. Before that, we run models that only vary initial plate ages for comparison with those that contain a hot region on the OP (Table A2). The naming of the models depends on the parameter types and is shown in Table A1 and A2.

Model SP90_OP20 ($AgeSP^0$ is 90 Ma and $AgeOP^0$ is 20 Ma) without a hot region was chosen as a reference model (RM, Figure 2) for testing properties of the hot region. The subducting plate (SP) sinks rapidly and reaches the boundary between the upper mantle (UM) and lower mantle (LM) at about 4 Ma after model initiation. During this time, the OP basement near the trench is eroded by the mantle wedge flow, and the region that is about 750 km away from the trench on the OP becomes thinner, a region which is under extensional stress (Figure 2d). After the SP tip reaches the LM which is more viscous compared to the UM, its subduction slows down due to the increased resistance, which leads to the subduction process becoming steady state (Capitanio et al., 2007). The eroded part and thinning region of the OP lithosphere heal gradually during the steady state subduction stage, after which time the whole OP is under a compressional environment. The trench retreats all the time though the rate of retreat varies. The models that tested the effect of the properties of the hot region are all set the same $AgeSP^0$ and $AgeOP^0$ with the RM (Table A1).

3.1 Back-arc extension modes

The extension levels on the OP are defined by the isothermal contour of 1300 K (Figure 3). The contour curving up means the OP is thinned in thermal structure, which is defined as 'Thinning' (Figure 3b). When the contour curve reaches the cold thermal surface, the OP finishes thinning (Complete Thinning, Figure 3c) and turns to spread (Figure 3d) which is named 'Spreading'. The stage when the thinning is completed is the critical point between Thinning and Spreading, after that the extensional state begins. Thus, we introduce two new classifications 'Extension' and 'No Extension' identified by capitalisation, where we classify Complete Thinning and Spreading as 'Extension' and the states before Complete Thinning as 'No Extension'.

Based on the above definition, three end-member modes of back-arc extension on the OP are recognised (Figure 4): (A) No Extension on the OP (NE), which means there is no actual spreading or thinning on the OP; (B) Extension at the Far-field location (around 750 km from the trench) which is far away from the hot region and the very same region where the thinning takes place in the RM (EF); (C) Extension at the Hot region (EH, EH-D). We also get the fourth mode (D) which has two (dual) extensions, i.e. at both places in modes B and C (EF+EH). The ones showing slab detachment after the back-arc extension have been subdivided into EH-D (Figure 4g, h), for the case in which the slab breaks off, in these cases, the plate loses its slab pull and both the subduction and trench retreat stops. The extension of all modes lasts for a short time (just 1 to several million years) and then heals gradually in the steady subduction state or after slab detachment (in EH-D mode).

The reason why we combine EH and EH-D into the same mode is that the slab detachment occurs after the back-arc extension and has no effect on driving the extension. The specific morphology is not the primary focus of this research.

https://doi.org/10.5194/egusphere-2023-1791
Preprint. Discussion started: 17 August 2023

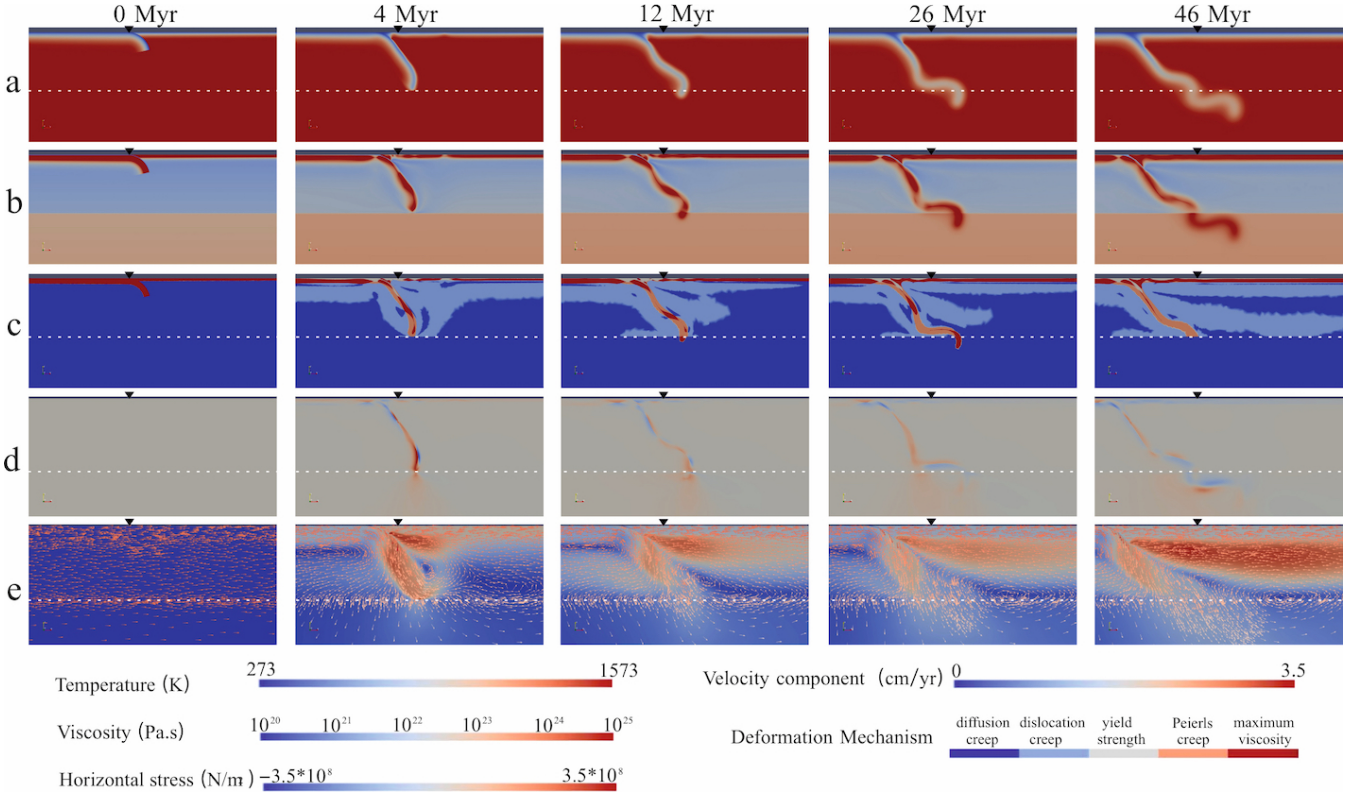

Figure 2. Simultaneous snapshots of a zoom in of the reference model showing the time evolution of (a) temperature field; (b) viscosity field; and (c) dominant deformation mechanism; (d) horizontal stress (positive value indicates extensional stress); and (e) the magnitude of velocity field with arrows. The black lower triangles mark the initial trench positions, and the dashed line represents the boundary of UM and LM.

3.2 Varying parameters of the hot region

More than 200 models have been performed by varying the following parameters of the hot region: the distance from the trench to the centre of the hot region (Distance), the width from the heated centre of the hot region to each side (Width), and the increased temperature at the centre of the hot region from the background temperature (ΔT)(shown in Figure 1 and Table A1), to investigate the influence of a pre-existing hot region (a volcanic arc) on back-arc extension.

3.2.1 Regime diagrams

In this section, we mainly show how the modes change through changes in the above parameters (Figure 5, 7).

Firstly, the Width was fixed to 50 km and the Distance and ΔT were tested systematically (Figure 5). All of the modes we introduced in section 3.1 are identified in this series of models. When the hot region is quite close to the trench, such as when

https://doi.org/10.5194/egusphere-2023-1791
Preprint. Discussion started: 17 August 2023

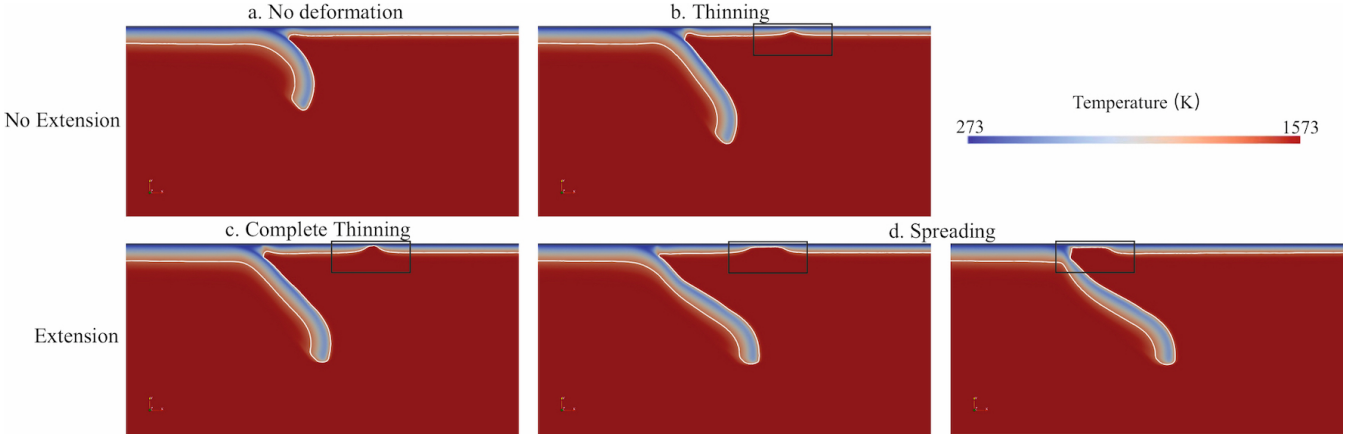

Figure 3. Defination of the extension levels by the isothermal contour of 1300 K (the white line). The temperature fields show (a) No deformation, (b) Thinning, (c) Complete thinning and (d) Spreading (far-field spreading on the left and hot-region spreading on the right). (a) and (b) are classified as 'No Extension', whereas (c) and (d) are classified as 'Extension'.

the Distance is 100 km, the model behaves as mode NE (No Extension) no matter how hot the hot region is. As the hot region is emplaced farther away from the trench, an extension emerges at the far-field location (mode EF). When the ΔT is prescribed to 50 degrees, Extension cannot appear if the distance is less than 150 km. Whereas when the thermal anomaly is increased to 100 degrees, the Extension occurs even when the distance is only 130 km. In other words, the distance threshold controlling the emergence of Extension on the OP reduces as the temperature of the thermal anomaly increases.

As the distance increases further, the mode of the cases changes from EF to EH, which has Extension at the hot region close to the trench. The threshold of distance, controlling the transition from mode EF to EH, has the same trend as that controlling the existence of Extension. When the distance is larger than the threshold, most of the cases show mode EH as long as there is an Extension. However, model W50_Di1050_T50 (W50 means that the Width is 50km; Di1050 represents the Distance is 1050km; T50 means that the ΔT is 50 degrees) shows mode EF unexpectedly (Figure 6). In this model, the hot region is located at 1000-1100 km from the trench, but the Extension is still around 750 km from the trench. When the hot region is very close or very far away from the trench, the Extension could emerge near a distance of around 750 km from the trench.

To find out the role of the Width, we reduce it from 50 km to 25 km. A series of cases investigate how the combination of the Distance and ΔT changes the extension behaviour of the different-width hot region (Figure 7). The depth extent of the thermal anomaly has not been changed in these models. Compared to Figure 7a, the results in Figure 7b show that the thresholds between mode NE and EF, as well as mode EF to EH in distance and heating temperature both increase obviously. Take models with 100 degrees temperature increase for example, when the distance is 150 km, the model with a width of 50 km shows EF mode which has an Extension on the OP, but the model with a width of 25 km is in NE mode which does not show Extension on the OP. Regardless of the specific values, the tendency of the changes in threshold when the width is 25 km is the same as that with a width of 50 km. In summary, as one might expect, a wider hot region favours Extension.

https://doi.org/10.5194/egusphere-2023-1791
Preprint. Discussion started: 17 August 2023

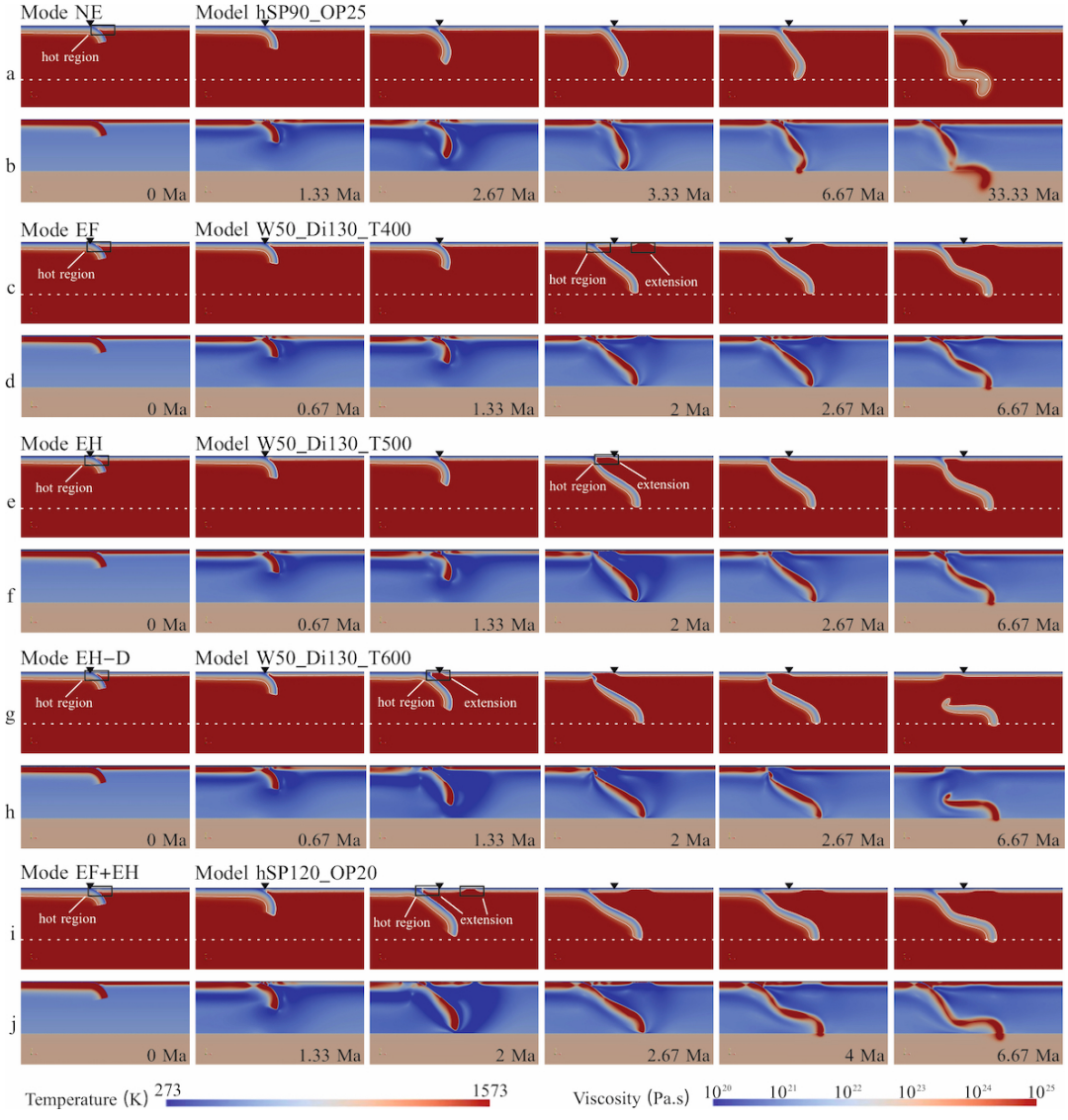

Figure 4. Four modes of the back-arc extension on the OP: (a)(b) NE; (c)(d) EF; (e-h) EH (including EH-D which shows slab detachment in (g)(h)); (i)(j) EF+EH. (a) (c) (e) (g) (i) show the temperature field with the isothermal contour of 1300 K in white, while (b) (d) (f) (h) (j) show the viscosity field, respectively. The parameters of each model are shown in Table A1 and S2. For example, in Model hSP90_OP20, $AgeSP^0$ is 90 Ma and $AgeOP^0$ is 20 Ma, 'h' means a hot region is included. W50_Di130_T400-600 means that Width is 50 km, Distance is 130 km, ΔT is 400, 500 and 600°C, respectively.

In conclusion, a farther distance from the heated centre to the trench, a higher temperature, and a larger size of the hot region all favour back-arc extension on the OP.

https://doi.org/10.5194/egusphere-2023-1791
Preprint. Discussion started: 17 August 2023

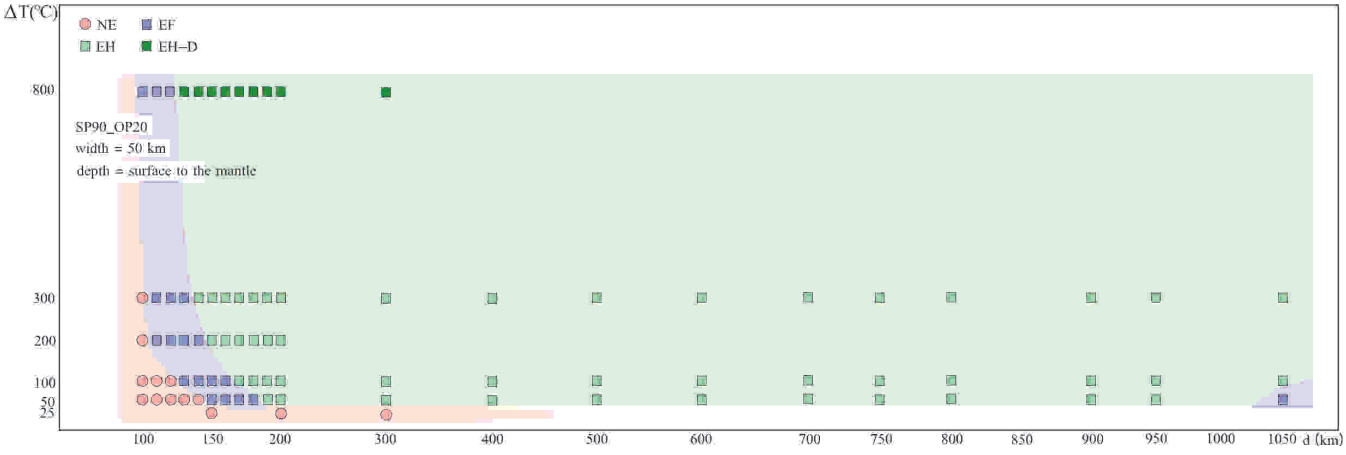

Figure 5. Regime diagram showing the Extension behaviour of the overriding plate with a hot zone. It is a function of the distance from the trench to the centre of the hot region (d, km) and the temperature anomaly of the hot region (ΔT). The width of the hot region is fixed at 50 km.

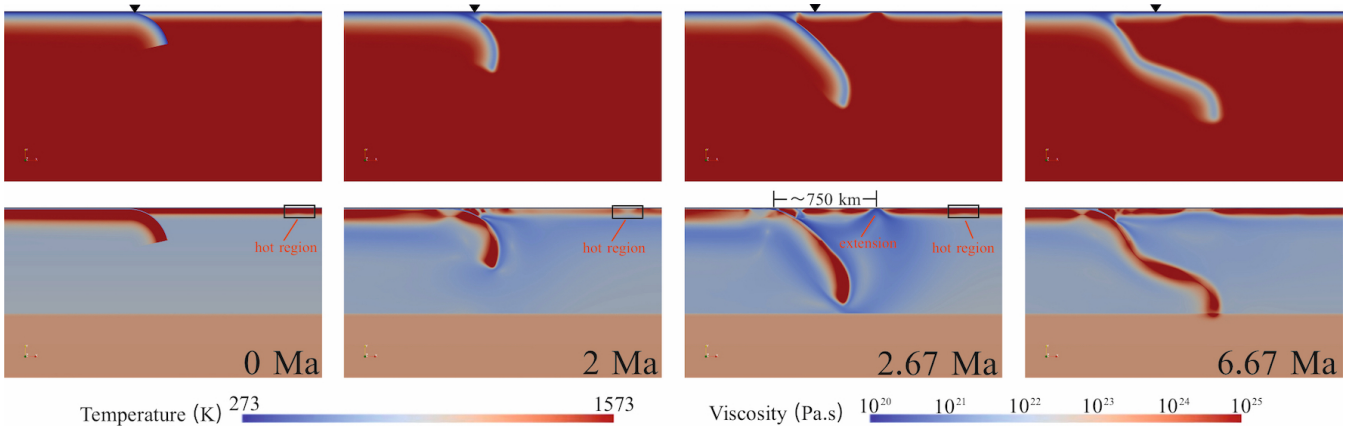

Figure 6. W50_Di1050_T50 in EF mode.

3.2.2 Correlation to the trench retreat rate

The vertical series of models with the Distance value of 130 km in Figure 5 are chosen to investigate the influence of the ΔT. The ΔT varies from 50 to 800 degrees, and the modes that they show transfer from NE to EF, then to EH as the ΔT increases.

As stated in the description of the Reference Model (RM), the SP sinks rapidly initially, accelerating until the tip reaches
185 the transition zone between the UM and the LM. After introducing a hot region into the OP, the SP sinks more rapidly on average and the trench retreats slightly faster before the SP reaches the lower mantle than in the RM. When the ΔT increases, the general SP rate rises as well, and the SP tip takes less time to get to the transition zone (Figure 8b). Like the vertical SP

https://doi.org/10.5194/egusphere-2023-1791
Preprint. Discussion started: 17 August 2023

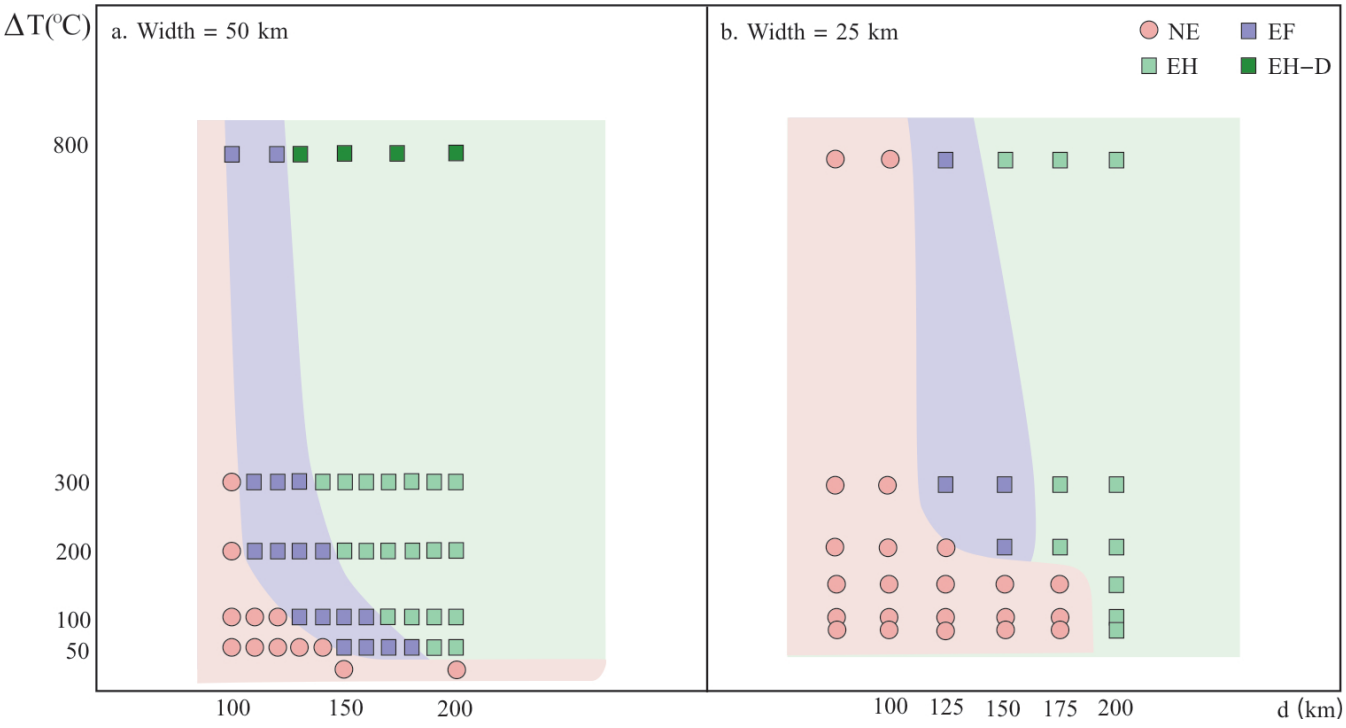

Figure 7. (a) Regime diagram of distance vs. ΔT when the width is 50 km and (b) the comparison to the results when the width is 25 km.

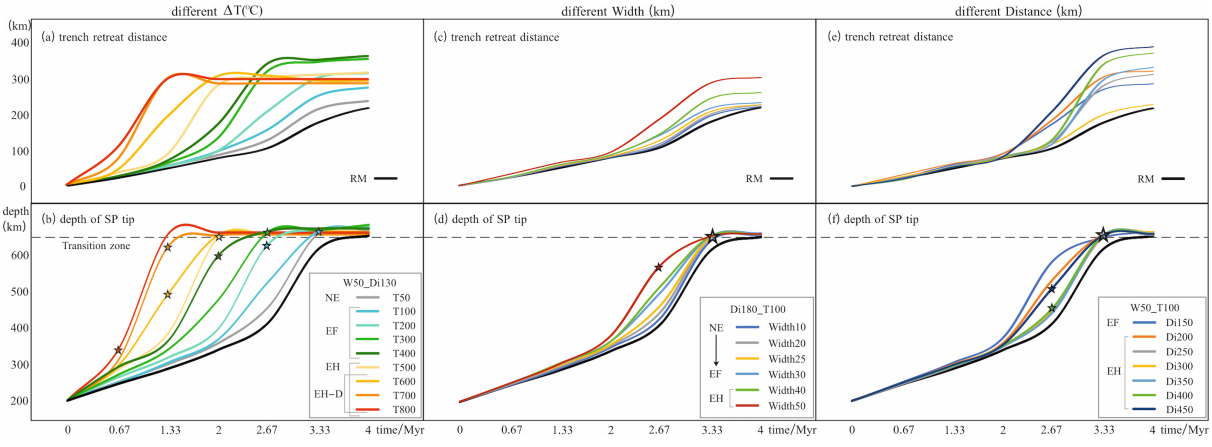

Figure 8. Comparisons of total (a) (c) (e) trench retreat and (b) (d) (f) depth of SP tip subduction throughout the first 4 Myr simulation with various ΔT (a, b), different Width (c, d) and various Distance (e, f), respectively. The grey dashed line represents the transition zone depth (660 km). The stars mark the time when the Extension occurs in each model, and the colour of the stars is the same as the lines of each model.

https://doi.org/10.5194/egusphere-2023-1791
Preprint. Discussion started: 17 August 2023

rate, the trench retreat rate shows a similar trend as ΔT increases (Figure 8a). When the ΔT is no more than 400 degrees, the trench retreats at a similar speed at first, then the model with a hotter 'arc' shows a quicker trench retreat, after 3.33 Myrs, the trench keeps quite a slow retreating rate in the steady state stage. As the ΔT is increased further, the trench obviously retreats faster before the SP reaches the transition zone. The trench stops retreating after the slab detachment in Mode EH-D, because there is no extra force exerted on the SP.

Similarly, when the Width rises, both the SP rate and trench retreat rate slightly increase with the same trend as when ΔT increases (Figure 8c, d), though the increase with Width is much less than with ΔT. However, there is no specific correlation between Distance and trench retreat rate (Figure 8e) / SP sinking rate (Figure 8f). For example, compared to model W50_T100_Di300 showing the slowest trench retreat rate except for the RM, the trench in model W50_T100_Di200 retreated more quickly and farther until 4 Myrs.

Whether increasing the Width or ΔT, the hot region is hotter and weaker in total, which encourages the trench retreat even though the ultimate controlling mechanism is still unclear. Whereas varying the Distance alone has no influence on the trench retreat since the heated area and temperature are unchanging. Besides, the EH-D did not occur in the two latter series of models, which possibly means that the ΔT has the most significant influence on the behaviours of the plates.

3.3 Varying initial plate ages adjacent to the trench

We chose the hot region located 100-200 km from the trench and heated it by 200 degrees (the same as that in Model W100_Di150_T200), and tested how different combinations of plate ages influence the OP deformation (Table A2). The results of changing the initial OP age and SP age at the trench, showing the modes of the OP deformation, are shown in Table A2 and Figure 9. In general, the figure reveals that older SP age tends to result in Extension when the OP age remains unchanged, whereas a younger OP age leads to Extension when the SP age is fixed.

In models without a hot region (modes changing shown by the dashed line), when the initial age of the OP adjacent to the trench ($AgeOP^0$) is prescribed to be 20 Ma, the threshold of the initial age of the SP at the trench ($AgeSP^0$) that leads to Extension is 100 Ma (Model SP100_OP20), and a little bit of thinning occurs at the place where Extension exists in Model SP100_OP20 if the $AgeSP^0$ is decreased to 90 Ma (Model SP90_OP20). We change the $AgeOP^0$ and find the minimum $AgeSP^0$ to generate Extension for each $AgeOP^0$. As seen in Figure 9, model SP60_OP15, SP95_OP20, SP165_OP25, and SP280_OP30 are the marginal cases in the region in which the models have Extension. As $AgeSP^0$ increases from 70 Ma to 280 Ma, the time before Extension occurs gets slightly longer, from 2.7 Ma to 4.7 Ma. For these three models, increasing $AgeOP^0$ or decreasing $AgeSP^0$ stops Extension. All of this extension or thinning happens at a far-field location about 700-750 km from the trench.

Adding a hot region increases the age threshold of the existence of Extension, which is shown by the boundary of the pink area and the dashed line (Figure 9), and allows Extension to occur at the hot region which is much closer to the trench than the far-field location. When the $AgeSP^0$ is relatively young, Extension is more likely to happen at the arc, though some cases showed far-field Extension before adding the hot region (eg.SP80_OP15 and hSP80_OP15, 'h' in the model name means a hot region is set in the model). Most models with an $AgeSP^0$ older than 100 Ma tend to lead to an EF mode. Furthermore, the

https://doi.org/10.5194/egusphere-2023-1791
Preprint. Discussion started: 17 August 2023

transition modes in Figure 9 show how the end-member modes change when the initial plate ages near the trench vary. Take the OP20 series of models for example, when the $AgeSP^0$ increases from a low value (such as hSP60_OP20 which is mode NE), Extension first occurs at the hot region (eg.hSP70_OP20; mode EH) and at the far-field location (mode EF) when $AgeSP^0$ is old enough (eg.hSP150_OP20). Transitional mode EH+EF is shown in this process as well.

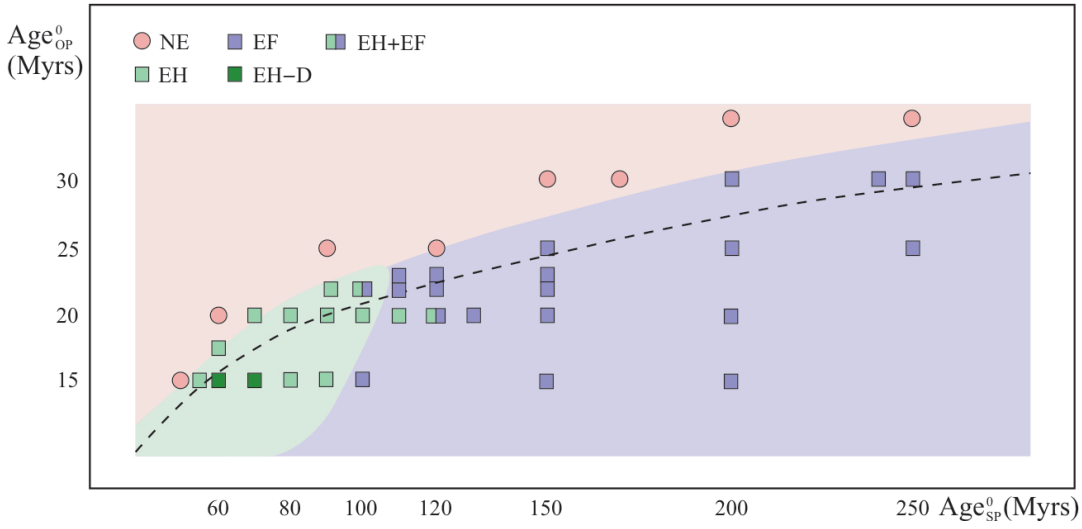

Figure 9. Regime diagram of the combination of $AgeOP^0$ and $AgeSP^0$. Each symbol represents a model with a hot region located from 100 to 200 km from the trench, and the different colour regions are classified by the results of models with a hot region. For comparison, the threshold for the existence of extension in models without a hot region is marked by the black dashed line. Note that one symbol with two squares means two end-member modes both happen in one model.

4 Discussion

4.1 The driving mechanism of the back-arc extension

Generally speaking, back-arc extension can be driven by an extensional force related to plate motions or/and subduction-induced mantle flow in a subduction zone. In the first mechanism, the extensional force is generated from the speed difference of the plates, and it can be reflected in the horizontal stress field (Figure 10). Mantle flow is shown as only poloidal flow in our 2D section.

The analysis of the horizontal stress shows a compressional region close to the trench just before the Extension occurs in all the models (Figure 10), which is consistent with that in RM (Figure 2d) and some previous numerical models (Chen et al., 2016; Schellart and Moresi, 2013). Even though Extension in Mode EH occurs near the trench (orange star in Figure 10), the vertically integrated horizontal stress (Σ_h) shows no observable difference from that in EF mode. It even seems that the EH happens in a compressional zone, which might be because the extensional period before the compression is too short to be

https://doi.org/10.5194/egusphere-2023-1791
Preprint. Discussion started: 17 August 2023

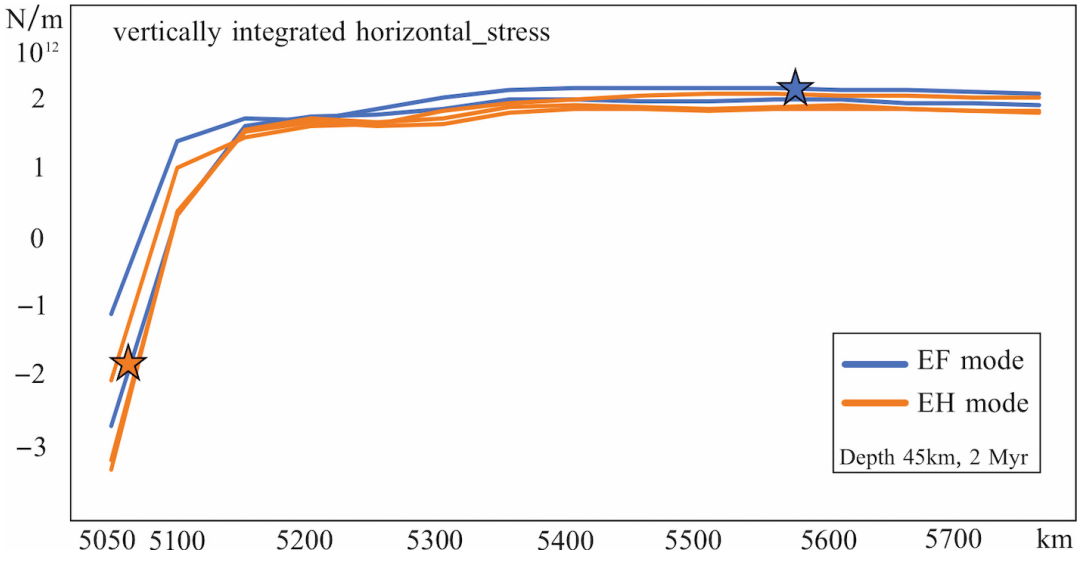

Figure 10. Vertically integrated horizontal stress over OP thickness (from the surface to the OP bottom, 45 km depth, which was defined by the temperature contour of 1300K) vs. x coordinate (the trench starts with an x coordinate of 5000 km). A positive stress value means extensional. For clarity, only two colours are used in this figure to represent models in different modes (see legend). The chosen models are W50_Di120_T100 and W50_Di150_T100 which are in EF mode; W50_Di170_T100, W50_Di190_T100, and W50_Di250_T100 which are in EH mode. Stars mark locations of back-arc extension in the same colour as their plots (eg. blue star represents the extensional location in EF mode), respectively. This is evaluated after 2 Myr in all simulations.

output under the output timestep we use in these models. The introduction of the hot region has almost no influence on Σ_h. Therefore, the change of Σ_h does not really decide if Extension occurs, which means that the horizontal extensional force can be ignored as a cause of Extension in our models.

The RM shows only very limited thinning at approximately 750 km away from the trench on the OP (Figure 2). To produce back-arc extension, either the OP needs to weaken or the driving force needs to increase. In this series of models, the OP can be weakened in two ways. One is through the hot zone which was introduced in the initial setup, because viscosity decreases as temperature rises (Eq. (6)), the hot zone would be easier to extend; the other way it could be weakened is by upwelling flow beneath the OP. This latter process must have occurred in this series of models, as implied by the existence of the EF mode. In total, the main driving mechanism is poloidal flow induced by the SP tip and shown by the velocity field (Figure 11). The trench-ward horizontal flow (X component) produces basal drag by the velocity gradient (Figure 12), whereas the upwelling thermal intrusion (Y component) weakens the OP to facilitate an Extension. The upwelling flow is always in a similar direction (about 60° to the horizontal) so it approaches the OP. The horizontal size of the upwelling flow cell varies a little, is around 750 km (± 80 km) in the horizontal direction, largely as a result of the varying SP dip/morphology arising from varying slab retreat rates. This far-field location is regarded as the edge of the flow cell in this work.

https://doi.org/10.5194/egusphere-2023-1791
Preprint. Discussion started: 17 August 2023

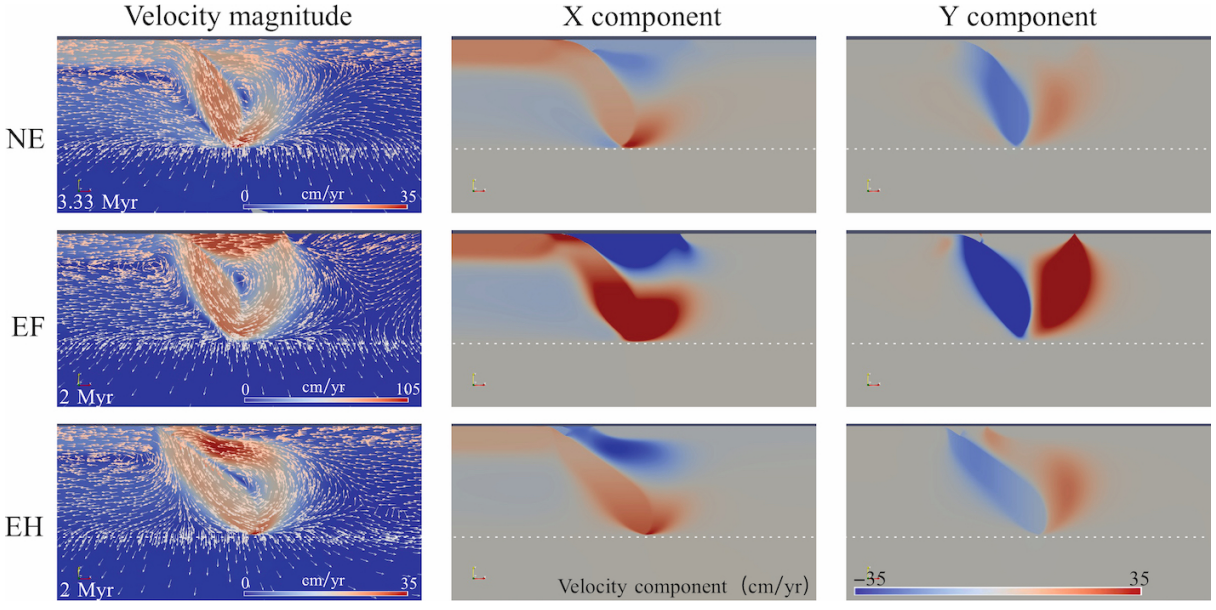

Figure 11. Velocity fields in 3 modes. The arrows indicating the direction of the mantle flow are marked in the magnitude velocity field. In the velocity component field, the positive value represents rightwards (in the x component field) or upwards (in the y component field). The chosen time is just before the Extension (in Mode EF and EH) or Thinning (in Mode NE). Note that the scale of Velocity magnitude in Mode EF is set three times larger than that in other modes to improve figure clarity.

The Extension process is the competition of basal drag which thins the OP versus thermal healing which thickens it. The model goes to rift when the basal drag wins out, but thermal healing is always efficient because all models showing Extension show it healing after a few Myrs of Extension as well. The thermal weakening starts at the base of the thermal boundary between the OP and the underlying mantle, though the viscosity weakens from both the base and the top of the OP (Figure 4) and produces 'necking' (Lei, 2022) in the middle, which is because yielding viscosity dominates at the top and it is not dependent on the temperature but on the yielding strain rate and the depth. Then the Extension appears from the base of the OP and the material flows into the gap at the surface. Thermal thinning gives thermal weakening, equally the hot region provides thermal thinning at the start of such simulations and encourages Extension.

4.2 The role of an existing arc

In numerical models, the existence of an arc is not necessary to produce Extension in the OP (Figure 9; Sheng et al., 2019 and other references). However, the position of the Extension depends on the size of the mantle flow cell (about 750 km in our models) if the OP is homogeneous. A hot region on the OP not only facilitates the Extension to happen but also changes the position of the Extension under some conditions (Figure 5, 9). The specific mode that a model produces depends on different parameters, including properties of the hot region and plate ages in our cases. There have been many studies investigating the

https://doi.org/10.5194/egusphere-2023-1791
Preprint. Discussion started: 17 August 2023

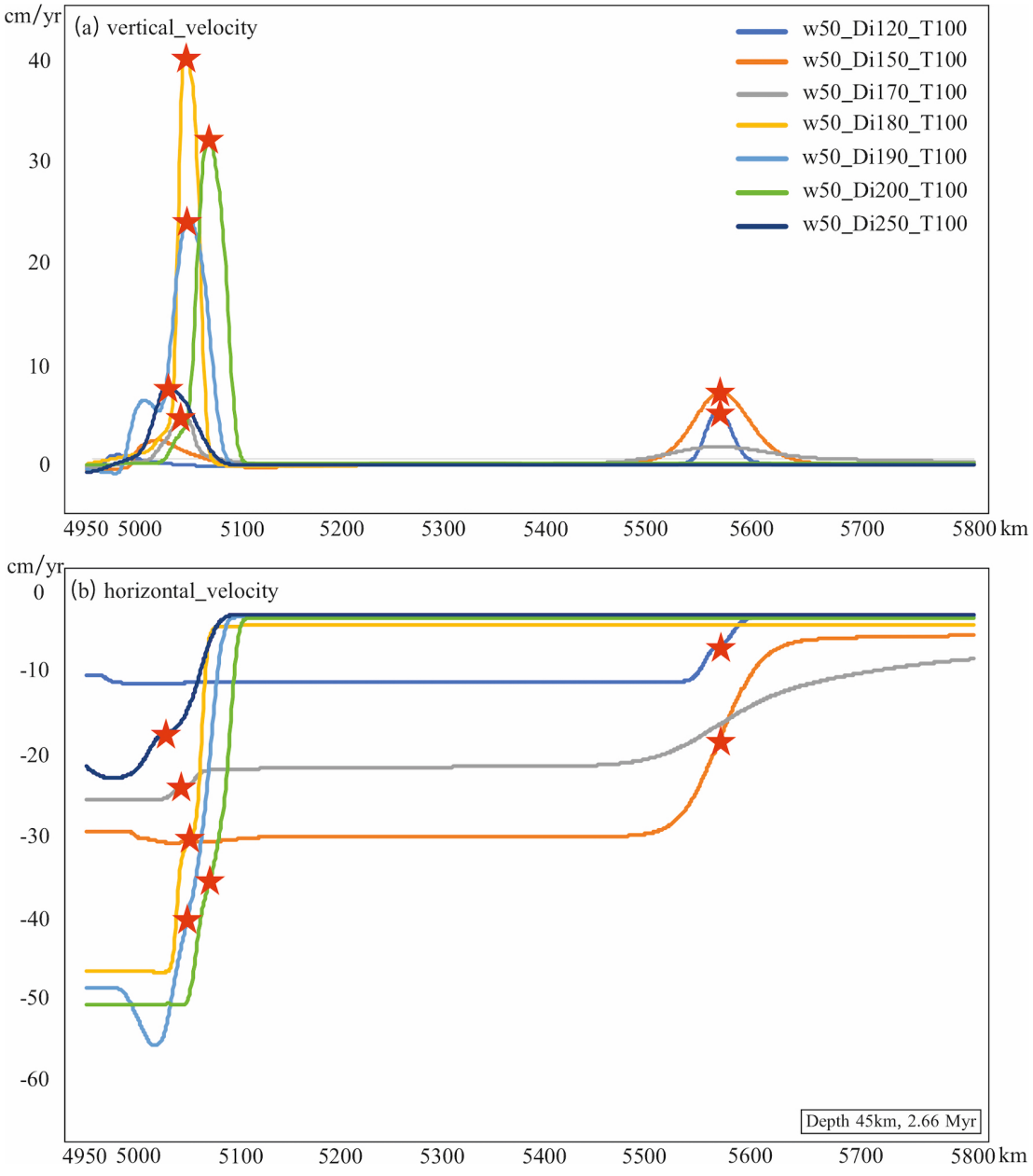

Figure 12. Velocity components vs. x coordinate at 45-km depth at 2.66 Myr. (a) Vertical velocity (Y component) vs. x coordinate; (b) Horizontal velocity (X component) vs. x coordinate. The back-arc extension is marked by red stars. Models W50_Di120_T100 and W50_Di150_T100 are in Mode EF, the others are all in Mode EH.

265 role of plate ages on back-arc extension (Sdrolias and Müller, 2006; Capitanio et al., 2011; Sheng et al., 2019; Dasgupta et al., 2021) or slab/plate behaviours (Garel et al., 2014), so details will not be discussed in this study.

https://doi.org/10.5194/egusphere-2023-1791
Preprint. Discussion started: 17 August 2023

When the plate ages are fixed and the model shows Thinning but no Extension before a hot region is introduced, some models show Extension at the hot region (Mode EH), which means the hotter and weaker 'arc' is split apart; whereas some others show Extension at the same place as the thinning location even though the weakened zone is much closer to the trench (Mode EF), which implies the driving force (including the force which weakens the OP) is undoubtedly enhanced.

The Extension process is a competition of thermal weakening at the hot region and at the far-field location. The former is mainly from the thermal thinning of the hot region itself, so it depends on the Width and ΔT (the viscosity is dependent on temperature which is shown in Eq.6). The latter is from the mantle wedge flow, which is controlled by initial plate ages and Width and ΔT as well because faster trench retreat (Section 3.2.2) induces a stronger mantle flow (Lei, 2022). The results show the contribution that Width and ΔT make to the thermal weakening of the hot region is greater than that to the wedge flow. The thermal weakening draws in some flow because of the continuity of mass, which makes the hot region weaker and encourages more Extension. At the same time, the weakening accelerates the trench retreats and induces more wedge flow. When the mantle flow is firstly strengthened, the place which concentrates the flow at the far-field location is weakened and dragged by stronger basal traction no matter where the weak region is, which results in Mode EF. However, when the Width and ΔT are high enough, the thermal weakening in the hot region dominates the process, and the hot region becomes the region of Extension, which is Mode EH (Figure 11). At the same time, the flow going to the far-field location reduces because the upwelling focuses on the hot region, so the far-field location does not show Extension anymore. If the thermal thinning which the mantle wedge flow produces exceeds that produced by the hot region, then Extension occurs at the far-field location.

Different from the Width and ΔT, the Distance influences neither the trench retreat rate nor the size of the mantle flow. The upwelling flow is sucked into the edge of the flow cell and gradually decreases to each side (Figure 11). When the Distance increases, the hot region initially gets close to the cell edge and gains more upwelling intrusion. Hence, the hot region is increasingly weakened and attracts the mantle flow to itself. As the Distance increases further, the hot region moves away from the cell edge, and the mantle flow fades away, so Model W50_Di1050_T100 changes to EF mode again (Figure 6). However, a larger trench-arc distance is always associated with a flatter slab in nature (Cross and Pilger Jr, 1982), and there are positive correlations between the slab dip and back-arc extension so that a BAB would be rarely observed when the arc is relatively far away from the trench.

Figure 9 shows that when $AgeSP^0$ is relatively young (eg. 60-90 Ma), some cases which have an Extension at 750 km away from the trench with a homogeneous OP generate EH mode after adding the hot region. In these cases, a hot region largely weakens the OP and concentrates the flow at the weak zone though the arc also facilitates the mantle flow. When the arc is much easier to be broken than the far-field location for this mantle flow, the flow tends to focus on the arc and the far-field location loses the extensional stress. The high negative buoyancy and strength of an older SP encourage a higher trench retreat rate and a stronger mantle flow (Garel et al., 2014), so that the flow is strong enough to break at the far-field location before the weak zone is broken. Under such circumstances, the models show EF mode.

https://doi.org/10.5194/egusphere-2023-1791
Preprint. Discussion started: 17 August 2023

4.3 Comparison to observations in nature

Mode NE (No Extension), Mode EH (Extension at the Hot region) and Mode EF (Extension at Far-field location) are identified as three end-member modes (Section 3.1). In nature, similar behaviours to Mode NE and Mode EH are shown in many subduction zones. For example, the Lesser Antilles subduction zone does not show back-arc extension on the OP (Caribbean Plate), which is consistent with Mode NE. The phenomenon that many BABs were formed by splitting a volcanic arc apart (Mariana Trough, Lau Basin, East Scotia Basin, etc) is reproduced by Mode EH. However, very few or even no BAB is definitely observed extending far away from the volcanic arc (like the Mode EF process). Speculating from the limited available information, the Japan Sea possibly formed far away behind the Japan Arc (Tatsumi et al., 1990) and might be an EF example. It is observed that the Japan Arc is approximately 300 km away from the Japan Trench (Jarrard, 1986), and the distance from the spreading centre of the Japan Sea to the trench is around 700 km (Tamaki, 1992), which is close to the mantle flow size in our models (750 km). Admittedly, there are opinions claiming that the Japan Sea opened at a proto-Japan Arc (Jolivet et al., 1994), but the evidence presented is debatable due to the lack of a remnant ridge on the western side of the Japan Sea.

Generally speaking, an old SP is more likely to generate back-arc extension in our models, which is consistent with observations in nature. For example, the East Pacific SPs are quite young at the interface where entering the subduction zones, corresponding to which there are few BABs found along the East Pacific margin. Specifically, the Juan de Fuca, the Explorer, the South Gorda and the Winona plates, which are along North America, are less than 10 Ma (Rogers, 1988), and the Nazca Plate which subducts beneath the South American Plate is about 40 Ma (Capitanio et al., 2011). In contrast, most western Pacific SPs are older than 100 Ma (Müller et al., 2008), and there are a lot of BABs distributed along that margin. This phenomenon meets our basic model behaviour. However, our models show Mode EF when the SP age is quite old because of the strong mantle flow it induces, whereas most of the BABs along the western Pacific formed in the process of Mode EH. To generate an EH, our models require an SP aged less than about 100 Ma and a young OP, or a hot region with a large size and high temperature when the SP is relatively old. In view of the ages of the western Pacific SPs (over 100 Ma), it is assumed that the arcs in nature would be hotter than that in our models. Unfortunately, the uncertainty in the effects of actual arcs on back-arc extensions makes it difficult to compare our model directly with observations.

Besides, the survival time of the extensions in our models is consistent with that in nature. Real back-arc basins are not active for a long time, mostly the Extension duration lasts less than 20 Myrs. For example, ^{40}Ar-^{39}Ar dating indicated that the basement of the Japan Basin was aged 24-17 Ma, which means the crust grew for 7 Myrs (Kaneoka, 1992). The ages of the present-day BABs are usually less than 10 Myrs, like the Mariana Trough started 5 Myrs ago, the Okinawa Trough is only 2 Ma, and the Lau Basin has been active for 7 Myrs. The models of both EF and EH show that the Extension stops and tends to heal its thermal structure within 4-15 Myrs (older SP keeps the Extension longer), which is consistent with some cases in nature (eg. the Sulu Sea lasted for about 4 Myrs and Vavilov Basin lasted for 3-4 Myrs; Schliffke et al., 2022).

We must also acknowledge that the properties that a given arc would present to an overriding plate, in simulations like ours, is currently poorly defined. This further complicates, for now, a detailed comparison between models and nature.

https://doi.org/10.5194/egusphere-2023-1791
Preprint. Discussion started: 17 August 2023

4.4 Limitations

1. 2D modeling. (1) 2D models lack the lateral dimension of the real 3D world, which means the toroidal component of the mantle flow is ignored. There is some research suggesting that toroidal flow makes an important contribution to back-arc extension on the OP (Clio and Pieter, 2013); (Chen et al., 2016), especially at narrow subduction zones (Schellart and Moresi, 2013). The hypothesis of our 2D models is that the width of plates is infinitely wide and everywhere is the same along the third dimension. Thus, the models may not be applicable to the narrow subduction system, such as Gibraltar and the Calabria subduction zones. (2) We are implicitly assuming that the arcs are linear and constant along strike, while in reality the arc volcanoes focus along strike. (3) The plates can be inhomogeneous perpendicular to strike, a direction which is modelled, but only with simply varying plates to allow comparison, or along strike, a direction that is not modelled.

2. Simplification of the models. (1) We did not run models with a real continental OP, even though the Japan Sea, a case with a continental OP, is discussed in this paper. Because the models are simplified to include only mantle (more viscous than crust at the same temperature) viscosity, the OP lithosphere is stronger than it should be at a given age (the thermal structure depends on the initial age of plates). A younger age reduces the OP thickness and decreases the total strength to partly counteract the lack of crust. As a result, the same phenomenon requires a real plate to be older than that in our models (and even older age for a continental plate compared to an oceanic plate). (2) History of evolution is simple and similar to allow comparison across models, but this might be important in actual cases. (3) We have used a simple far-field boundary condition on the OP of a ridge, actual settings might be better represented by different boundary conditions. We have kept the models simple in this case to allow comparison. (4) The process of forming an arc is part of the subduction process, therefore, there is a possibility for important feedback between the arc and subduction that we cannot capture in these models.

5 Conclusions

Our models show that a volcanic arc has a significant impact on the back-arc extension on the OP in a subduction system even though extension can also happen without the arc.

1. By means of introducing a hot region on the OP and testing various parameters, three end-member types of back-arc extension are depicted: (a) No back-arc Extension on the OP (Mode NE); (b) back-arc Extension occurs at the far-field location (about 750 km from the trench, Mode EF); and (c) back-arc Extension at the Hot region (Mode EH), including models with slab Detachment (EH-D). NE and EH modes are common in nature, whereas EF mode is very rare. We speculate that the Japan Sea might be a case of EF mode.

2. Properties of the hot region influence the modes. A farther distance from the hot region centre to the trench (Distance), a larger width of the hot region (Width), and a higher increased temperature of the hot region centre (ΔT) encourage back-arc extension on the OP, as well as the modes transfer from (a) Mode NE, to (b) Mode EF, to (c) Mode EH.

3. Plate ages are important parameters influencing the mode changes as well. When the OP is homogeneous, an old SP or a young OP in a model encourages back-arc extension about 750 km from the trench on the OP (almost the same location as that in Mode EF). After introducing the hot region, we note that not only is back-arc extension more likely to happen, but the

https://doi.org/10.5194/egusphere-2023-1791
Preprint. Discussion started: 17 August 2023

Extension switches from its far-field location into the hot region itself in some modes with a relatively young SP ($AgeSP^0$ less than 100 Ma in our models, but this threshold age would change if the hot region varies).

4. The primary driving mechanism of our models is poloidal flow underneath the OP. The flow cell has almost the same size in every model, which focuses at around 750 km from the trench on the OP and gradually decreases towards the trench. A higher trench retreat rate facilitates the poloidal flow, thus encouraging back-arc extension.

Table A1: Models of SP90_OP20 with various hot region

Models	Width (km)	Distance (km)	ΔT (°C)	Mode
w50_Di100_T50	50	100	50	NE
w50_Di100_T800	50	100	100	NE
w50_Di110_T200	50	110	200	EF
w50_Di110_T300	50	110	300	EF
w50_Di110_T800	50	110	800	EF
w50_Di120_T50	50	120	50	NE
w50_Di120_T100	50	120	100	NE
w50_Di120_T200	50	120	200	EF
w50_Di120_T800	50	120	800	EF
w50_Di130_T50	50	130	50	NE
w50_Di130_T100	50	130	100	EF
w50_Di130_T200	50	130	200	EF
w50_Di130_T300	50	130	300	EF
w50_Di130_T400	50	130	400	EF
w50_Di130_T500	50	130	500	EH
w50_Di130_T600	50	130	600	EH
w50_Di130_T700	50	130	700	EH
w50_Di130_T800	50	130	800	EH
w50_Di140_T50	50	140	50	NE
w50_Di140_T100	50	140	100	EF
w50_Di140_T300	50	140	300	EH
w50_Di150_T50	50	150	50	EF
w50_Di150_T100	50	150	100	EF
w50_Di150_T300	50	50	300	EH
w50_Di160_T50	50	160	50	EF
w50_Di160_T100	50	160	100	EF
w50_Di160_T200	50	160	200	EH

https://doi.org/10.5194/egusphere-2023-1791
Preprint. Discussion started: 17 August 2023

w50_Di160_T300	50	160	300	EH
w50_Di170_T50	50	170	50	EF
w50_Di170_T300	50	170	300	EH
w50_Di180_T100	50	180	100	EH
w50_Di180_T300	50	180	300	EH
w50_Di190_T50	50	190	50	EH
w50_Di190_T300	50	190	300	EH
w50_Di200_T50	50	200	50	EH
w50_Di200_T800	50	200	800	EH
w50_Di400_T50	50	400	50	EH
w50_Di750_T50	50	700	50	EH
w50_Di750_T100	50	700	100	EH
w50_Di750_T300	50	700	300	EH
w50_Di800_T50	50	800	50	EH
w50_Di800_T100	50	800	100	EH
w50_Di800_T300	50	800	300	EH
w50_Di900_T50	50	900	50	EH
w50_Di900_T100	50	900	100	EH
w50_Di900_T300	50	900	300	EH
w50_Di1050_T50	50	1050	50	EF
w50_Di1050_T100	50	1050	100	EH
w50_Di1050_T300	50	1050	300	EH
w25_Di125_T200	25	125	200	NE
w25_Di125_T300	25	125	300	EF
w25_Di150_T200	25	150	200	EF
w25_Di150_T300	25	150	300	EF
w25_Di150_T800	25	150	800	EH
w25_Di175_T200	25	175	200	EH
w25_Di175_T800	25	175	800	EH
w25_Di200_T800	25	200	800	EH

Table A2: Models testing plate ages with/without a hot region

https://doi.org/10.5194/egusphere-2023-1791
Preprint. Discussion started: 17 August 2023

Models	SP age (Ma)	OP age (Ma)	hot region	Mode
SP55_OP15	55	15	N	NE
SP60_OP15	60	15	N	E
SP90_OP20 (RM)	90	20	N	NE
SP95_OP20	95	20	N	E
SP150_OP25	150	25	N	NE
SP160_OP25	160	25	N	NE
SP170_OP25	170	25	N	E
SP240_OP30	175	30	N	NE
SP275_OP30	275	30	N	NE
SP280_OP30	280	30	N	E
SP300_OP30	300	30	N	E
SP300_OP30	300	30	N	E
hSP55_OP15	55	15	Y	EH
hSP60_OP15	60	15	Y	EH-D
hSP60_OP18	60	18	Y	EH
hSP60_OP20	60	20	Y	NE
hSP70_OP15	70	15	Y	EH-D
hSP70_OP20	70	20	Y	EH
hSP80_OP15	80	15	Y	EH
hSP80_OP18	80	18	Y	EH
hSP80_OP22	80	22	Y	EH
hSP90_OP15	90	15	Y	EH
hSP90_OP22	90	22	Y	EH
hSP90_OP23	90	23	Y	NE
hSP90_OP25	90	25	Y	NE
hSP100_OP15	100	15	Y	EF
hSP100_OP20	100	20	Y	EH
hSP100_OP22	100	22	Y	EF+EH
hSP100_OP23	100	23	Y	NE
hSP110_OP15	110	15	Y	EF
hSP110_OP20	110	20	Y	EH
hSP110_OP22	110	20	Y	EF
hSP110_OP23	110	20	Y	EF

https://doi.org/10.5194/egusphere-2023-1791
Preprint. Discussion started: 17 August 2023

hSP120_OP15	120	15	Y	EF
hSP120_OP20	120	20	Y	EF+EH
hSP120_OP22	120	22	Y	EF
hSP120_OP23	120	23	Y	EF
hSP120_OP25	120	25	Y	NE
hSP130_OP20	130	20	Y	EF
hSP150_OP15	150	15	Y	EF+EH
hSP150_OP20	150	20	Y	EF
hSP150_OP22	150	22	Y	EF
hSP150_OP23	150	23	Y	EF
hSP150_OP25	150	25	Y	EF
hSP150_OP30	150	30	Y	NE
hSP200_OP15	200	15	Y	EF
hSP200_OP20	200	20	Y	EF
hSP200_OP25	200	25	Y	EF
hSP250_OP30	250	30	Y	EF
hSP300_OP30	300	30	Y	EF
hSP350_OP30	350	30	Y	EF

Code availability. The numerical simulations were run with the open-source and multiphase computational fluid dynamics code Fluidity (http://fluidityproject.github.io/). The code source of our models is available from the corresponding author upon reasonable request.

Author contributions. Duo Zhang: Writing the original draft & review & editing, Conceptualisation, Formal analysis, Investigation, Methodology, Visualisation, Validation, and Funding acquisition; Huw Davies: Writing - review & editing, Conceptualisation, Methodology, Validation, Supervision, Funding Acquisition, Project Administration, and Resources.

Competing interests. The contact author has declared that none of the authors has any competing interests.

Acknowledgements. This study is supported by PhD grant from Chinese Scholarship Council (No. 201906170045), Cardiff University and supercomputer Hawk in Cardiff University.

https://doi.org/10.5194/egusphere-2023-1791
Preprint. Discussion started: 17 August 2023

References

Bettina, B.-G., V, G. T., and Jean-Pierre, B.: Geodynamic regimes of intra-oceanic subduction: Implications for arc extension vs. shortening processes, Gondwana Research, 25, 546–560, 2014.

Capitanio, F. A., Morra, G., and Goes, S.: Dynamic models of downgoing plate-buoyancy driven subduction: Subduction motions and energy dissipation, Earth and Planetary Science Letters, 262, 284–297, 2007.

Capitanio, F. A., Faccenna, C., Zlotnik, S., and Stegman, D.: Subduction dynamics and the origin of Andean orogeny and the Bolivian orocline, Nature, 480, 83–86, 2011.

Chen, Z., Schellart, W. P., and Duarte, J. C.: Quantifying the energy dissipation of overriding plate deformation in three-dimensional subduction models, Journal of Geophysical Research: Solid Earth, 120, 519–536, 2015.

Chen, Z., Schellart, W. P., Strak, V., and Duarte, J. C.: Does subduction-induced mantle flow drive backarc extension?, Earth and Planetary Science Letters, 441, 200–210, 2016.

Clio, M. and Pieter, S. W.: Three-dimensional dynamic models of subducting plate-overriding plate-upper mantle interaction, Journal of Geophysical Research: Solid Earth, 118, 775–790, 2013.

Cross, T. A. and Pilger Jr, R. H.: Controls of subduction geometry, location of magmatic arcs, and tectonics of arc and back-arc regions, Geological Society of America Bulletin, 93, 545–562, 1982.

Dal Zilio, L., Faccenda, M., and Capitanio, F.: The role of deep subduction in supercontinent breakup, Tectonophysics, 746, 312–324, 2018.

Dasgupta, R., Mandal, N., and Lee, C.: Controls of subducting slab dip and age on the extensional versus compressional deformation in the overriding plate, Tectonophysics, 801, 228 716, 2021.

Davies, D. R., Wilson, C. R., and Kramer, S. C.: Fluidity: A fully unstructured anisotropic adaptive mesh computational modeling framework for geodynamics, Geochemistry, Geophysics, Geosystems, 12, https://doi.org/10.1029/2011GC003551, 2011.

Duarte, J. C., Schellart, W. P., and Cruden, A. R.: Three-dimensional dynamic laboratory models of subduction with an overriding plate and variable interplate rheology, Geophysical Journal International, 195, 47–66, 2013.

Erdős, Z., Huismans, R. S., and Faccenna, C.: Wide Versus Narrow Back-Arc Rifting: Control of Subduction Velocity and Convective Back-Arc Thinning, Tectonics, 41, e2021TC007 086, 2022.

Fowler, C. M. R., Fowler, C. M. R., and Fowler, M.: The solid earth: an introduction to global geophysics, Cambridge University Press, 1990.

Garel, F., Goes, S., Davies, D. R., Davies, J. H., Kramer, S. C., and Wilson, C. R.: Interaction of subducted slabs with the mantle transition-zone: A regime diagram from 2-D thermo-mechanical models with a mobile trench and an overriding plate, Geochemistry, Geophysics, Geosystems, 15, 1739–1765, 2014.

Holt, A. F., Becker, T., and Buffett, B.: Trench migration and overriding plate stress in dynamic subduction models, Geophysical Journal International, 201, 172–192, 2015.

Jarrard, R. D.: Relations among subduction parameters, Reviews of Geophysics, 24, 217–284, 1986.

Jodie, P.: Calculating arc-trench distances using the Smithsonian Global Volcanism Project database, https://www.earthbyte.org/calculating-arc-trench-distances-using-the-smithsonian-global-volcanism-project-database/, accessed April 27, 2023, 2016.

Jolivet, L., Tamaki, K., and Fournier, M.: Japan Sea, opening history and mechanism: A synthesis, Journal of Geophysical Research: Solid Earth, 99, 22 237–22 259, 1994.

Kaneoka, I.: ^{40}Ar-^{39}Ar analysis of volcanic rocks recovered from the Japan Sea Floor: Constraints on the age of formation of the Japan Sea, Proceedings of the Ocean Drilling Program, Scientific Results, 1992, 127, 819–836, 1992.

https://doi.org/10.5194/egusphere-2023-1791
Preprint. Discussion started: 17 August 2023

Kramer, S. C., Wilson, C. R., and Davies, D. R.: An implicit free surface algorithm for geodynamical simulations, Physics of the Earth and Planetary Interiors, 194, 25–37, 2012.

Lallemand, S., Heuret, A., and Boutelier, D.: On the relationships between slab dip, back-arc stress, upper plate absolute motion, and crustal nature in subduction zones, Geochemistry, Geophysics, Geosystems, 6, 2005.

Lei, Z.: Numerical investigation of the influence of subduction on deformation within the overriding plate, Ph.D. thesis, Cardiff University, 2022.

Magni, V., Faccenna, C., van Hunen, J., and Funiciello, F.: How collision triggers backarc extension: Insight into Mediterranean style of extension from 3-D numerical models, Geology, 42, 511–514, 2014.

Manga, M., Hornbach, M. J., Le Friant, A., Ishizuka, O., Stroncik, N., Adachi, T., Aljahdali, M., Boudon, G., Breitkreuz, C., Fraass, A., et al.: Heat flow in the Lesser Antilles island arc and adjacent back arc Grenada basin, Geochemistry, Geophysics, Geosystems, 13, 2012.

McKenzie, D. P., Roberts, J. M., and Weiss, N. O.: Convection in the Earth's mantle: towards a numerical simulation, Journal of Fluid Mechanics, 62, 465–538, 1974.

Müller, R. D., Sdrolias, M., Gaina, C., and Roest, W. R.: Age, spreading rates, and spreading asymmetry of the world's ocean crust, Geochemistry, Geophysics, Geosystems, 9, 2008.

Nakakuki, T. and Mura, E.: Dynamics of slab rollback and induced back-arc basin formation, Earth and Planetary Science Letters, 361, 287–297, 2013.

Rogers, G. C.: An assessment of the megathrust earthquake potential of the Cascadia subduction zone, Canadian Journal of Earth Sciences, 25, 844–852, 1988.

Schellart, W. P.: Quantifying the net slab pull force as a driving mechanism for plate tectonics, Geophysical research letters, 31, 2004.

Schellart, W. P. and Moresi, L.: A new driving mechanism for backarc extension and backarc shortening through slab sinking induced toroidal and poloidal mantle flow: Results from dynamic subduction models with an overriding plate, Journal of Geophysical Research: Solid Earth, 118, 3221–3248, 2013.

Schliffke, N., van Hunen, J., Allen, M. B., Magni, V., and Gueydan, F.: Episodic back-arc spreading centre jumps controlled by transform fault to overriding plate strength ratio, Nature Communications, 13, 582, 2022.

Sdrolias, M. and Müller, R. D.: Controls on back-arc basin formation, Geochemistry, Geophysics, Geosystems, 7, 2006.

Sheng, J., Li, C., Liao, J., Yang, Z., and Jiang, S.: Dynamics of back-arc extension controlled by subducting slab retreat: Insights from 2D thermo-mechanical modelling, Geological Journal, 54, 3376–3388, 2019.

Tamaki, K.: Tectonic synthesis and implications of Japan Sea ODP drilling, Tamaki, K., K. Suyehiro, J. Allan, M. McWilliams, et al, Proceedings of the Ocean Drilling Program, Scientific Results. Texas: College Station, 127, 2, 1992.

Tatsumi, Y., Maruyama, S., and Nohda, S.: Mechanism of backarc opening in the Japan Sea: role of asthenospheric injection, Tectonophysics, 181, 299–306, 1990.

Wolf, S. G. and Huismans, R. S.: Mountain building or Backarc extension in ocean-continent subduction systems: A function of backarc lithospheric strength and absolute plate velocities, Journal of Geophysical Research: Solid Earth, 124, 7461–7482, 2019.

Yang, S., Li, Z.-H., Wan, B., Chen, L., and Kaus, B. J.: Subduction-Induced Back-Arc Extension Versus Far-Field Stretching: Contrasting Modes for Continental Marginal Break-Up, Geochemistry, Geophysics, Geosystems, 22, e2020GC009 416, 2021.

Yang, T., Moresi, L., Gurnis, M., Liu, S., Sandiford, D., Williams, S., and Capitanio, F. A.: Contrasted East Asia and South America tectonics driven by deep mantle flow, Earth and Planetary Science Letters, 517, 106–116, 2019.

Zellmer, K. E. and Taylor, B.: A three-plate kinematic model for Lau Basin opening, Geochemistry, Geophysics, Geosystems, 2, 2001.